J. Fluid Mech. (2021), *vol*. 922, R3, doi:10.1017/jfm.2021.549

Experimental evidence of vortex-induced vibrations at subcritical Reynolds numbers

Pieter R. Boersma[1], **Jay Zhao**[1], **Jonathan P. Rothstein**[1] **and Yahya Modarres-Sadeghi**[1],†

[1]Department of Mechanical and industrial Engineering, University of Massachusetts, Amherst, MA 01003, USA

(Received 17 March 2021; revised 4 May 2021; accepted 14 June 2021)

Shedding of vortices can be observed in the wake of a fixed cylinder at Reynolds numbers larger than $Re = 47$. This might give the impression that a vortex-induced vibration (VIV), which occurs when the frequency of vortex shedding in the wake of a flexibly mounted cylinder synchronizes with the natural frequency of the structure, could be observed only at Reynolds numbers larger than $Re = 47$. Recent numerical simulations and theoretical work, however, have shown that it is possible to observe VIV at subcritical Reynolds numbers, i.e. Reynolds numbers smaller than $Re = 47$. In these studies, a VIV has been observed numerically at Reynolds numbers as low as $Re = 22$. In the present work, the first experimental evidence of VIV at subcritical Reynolds number is presented. We have designed and built an experimental set-up that makes it possible to conduct VIV experiments at subcritical Reynolds numbers, and at a constant Reynolds number over the entire lock-in range (i.e. the range for which oscillations are observed). Using this experimental set-up, we have confirmed experimentally that VIV can indeed be observed at subcritical Reynolds numbers, by observing VIV at Reynolds numbers as low as $Re = 19$. We have observed subcritical VIV both when the Reynolds number stays constant over the entire lock-in range, and when the Reynolds number increases with increasing reduced velocity, while staying within the subcritical range.

Key words: flow-structure interactions, vortex shedding, separated flows

1. Introduction

When the frequency of vortex shedding in the wake of a flexibly mounted cylinder free to oscillate in a direction perpendicular to the direction of incoming flow becomes equal to its natural frequency, the cylinder oscillates. These oscillations are observed for a range of reduced velocities (defined as $U^* = U/f_n D$, where U is the incoming flow velocity,

† Email address for correspondence: modarres@engin.umass.edu

f_n is the natural frequency of the structure and D is the cylinder's diameter), in which the oscillation frequency and the shedding frequency are synchronized. This range is called the lock-in range, and the oscillations that are observed within the lock-in range are called vortex-induced vibration (VIV). The vortex-induced vibration has been studied extensively both numerically and experimentally (Sarpkaya 2004; Williamson & Govardhan 2004; Païdoussis, Price & De Langre 2010), and over a wide range of Reynolds numbers, defined as $Re = UD/\nu$, where ν is the kinematic viscosity. Experimental studies on VIV of a cylinder have been conducted at Reynolds numbers larger than $Re = 47$, mainly because (i) for a fixed cylinder placed in flow, shedding of vortices starts at $Re = 47$ (Mathis, Provansal & Boyer 1984), and since VIV occur as a result of shedding of vortices in the wake of a cylinder, one would expect to observe VIV at Reynolds numbers larger than $Re = 47$, and (ii) conducting VIV experiments at relatively large Reynolds numbers (larger than $Re = 47$) is easier from a practical point of view. Recent numerical and theoretical studies, however, have shown that VIV can be observed at Reynolds numbers smaller than $Re = 47$. Buffoni (2003) showed experimentally that vortex shedding can be induced in the wake of a cylinder at Reynolds numbers as low as $Re = 25$ if the cylinder is forced to oscillate. Following this observation, Mittal & Singh (2005) conducted a numerical study on a cylinder in flow which is free to oscillate in both the cross-flow (CF) and inline (IL) directions, and observed VIV for Reynolds numbers as low as $Re = 20$. They used a global linear stability analysis and reported lock-in for both fixed and varying subcritical Reynolds numbers. Kou *et al.* (2017) used the dynamic mode decomposition approach and showed that the stable von Kármán mode almost completely vanishes for $Re < 18$, indicating that this could be the lower bound of the Reynolds number to observe VIV. Dolci & Carmo (2019) showed the subcritical nature of the bifurcation from steady to time periodic flow for reduced velocities within the lock-in range of a cylinder undergoing VIV, as opposed to the supercritical bifurcation observed for a fixed cylinder or for reduced velocities outside the lock-in range. They showed that the mass ratio and the number of degrees of freedom in the system do not influence this conclusion. Bourguet (2020) extended the numerical observation of VIV in subcritical Reynolds numbers to flexible cylinders, by observing VIV in a simply supported cylinder at Reynolds numbers as low as $Re = 20$, where higher modes of the flexible cylinder were excited as well.

Although numerical results and stability analyses have shown VIV in subcritical Reynolds numbers, no experimental work exists yet to confirm the existence of VIV at Reynolds numbers smaller than $Re = 47$. Also, in experimental studies, typically the reduced velocity is varied by increasing the flow velocity over a desired range, thus changing the Reynolds number as the reduced velocity is varied. In the current work, we report the results of a series of experiments that we have conducted to provide experimental evidence on the existence of VIV at subcritical Reynolds numbers, for both fixed and variable Reynolds numbers.

2. The experimental set-up

In order to be able to conduct a series of experiments to observe VIV at subcritical Reynolds numbers, we designed and built a rotating water channel with the goal of obtaining low flow velocities (figure 1*a*). The walls of this water channel consisted of two concentric acrylic cylinders with radii of $R_1 = 30$ cm and $R_2 = 25.4$ cm that were bonded to a flat circular acrylic plane. This plane was attached to a turntable which could rotate at a low angular velocity by a high torque electric motor attached to the centre of the plane. The rotational velocity of the motor was controlled by a variable voltage motor controller. The concentric cylinders created a channel with a width of $W = 4.6$ cm.

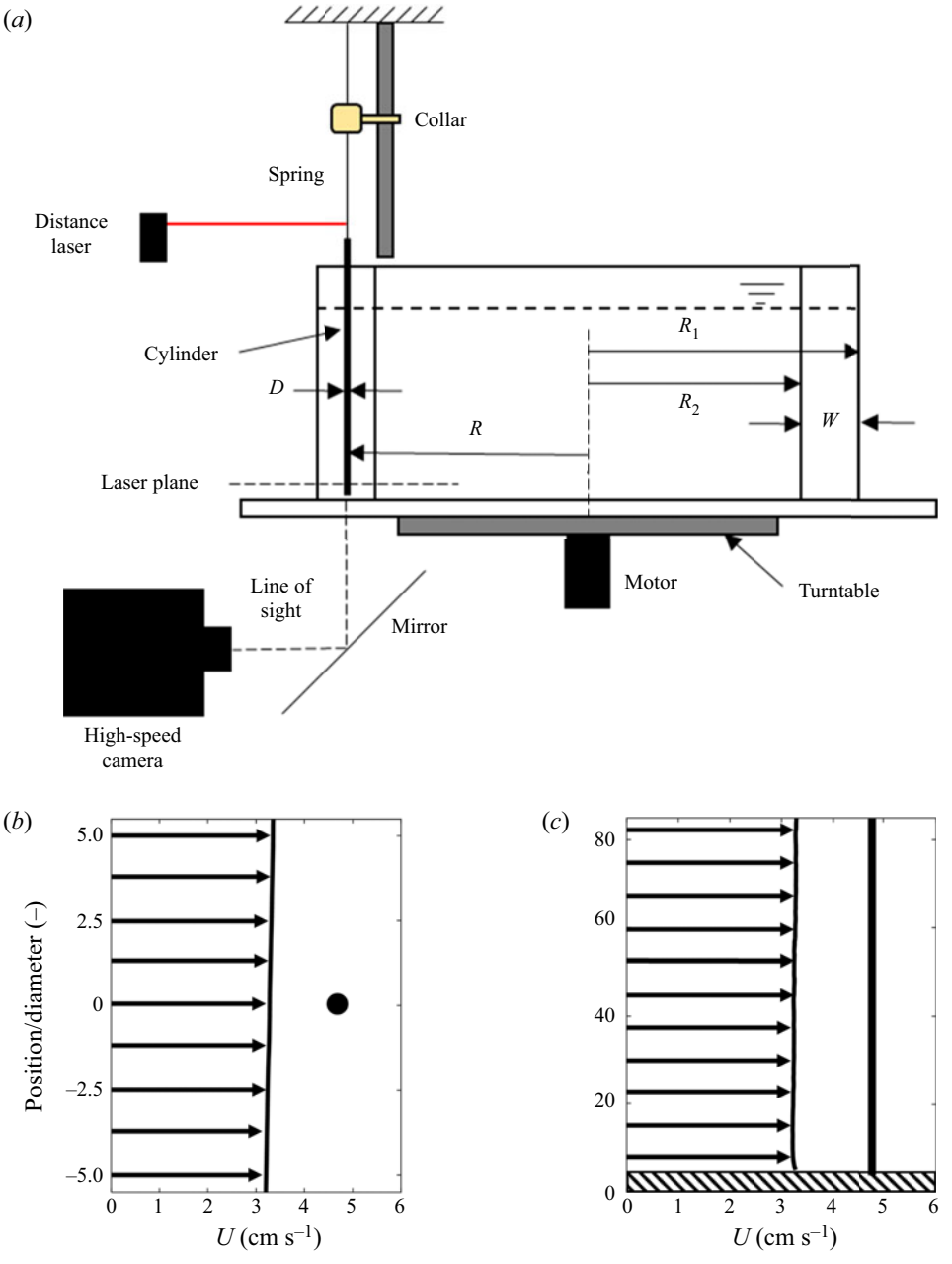

Figure 1. (*a*) A schematic of the water channel, the flexibly mounted cylinder, and the locations of the measurement devices, and samples of the measured flow profile at a flow velocity of $U = 3.3$ cm s^{-1}, corresponding to $Re = 33$ in the (*b*) horizontal and (*c*) vertical directions.

The use of clear acrylic for the sides and bottom of the channel allowed for the flow and the structure placed in the test section to be observed from any angle. Flow was created by rotating the water channel at given angular velocities. The water channel was capable of producing flow velocities in a range of $U = 1.5$ to 9.1 cm s^{-1} in increments of 0.1 cm s^{-1}. The flow velocity profiles at different flow velocities were measured using particle image

velocimetry (PIV), and it was found that the flow profiles were uniform, with a flow uniformity index ($|U - U_{ave}|/U_{ave}$, where U_{ave} is the mean value of the measured flow velocity) of around 0.037 ± 0.021 for the horizontal flow profiles and 0.003 ± 0.002 for the vertical flow profiles. Sample horizontal and vertical flow profiles for one of the flow velocities used in the present experiments, 3.3 cm s^{-1} ($Re = 33$), are shown in figure 1(*b*,*c*). These flow profiles were calculated by averaging the flow velocity at fixed points along the channel's width or height for 500 PIV frames.

To obtain a low Reynolds number, we placed a relatively small rigid cylinder with a diameter of $D = 1$ mm at the centre of the channel. The cylinder was held by a long thin piece of steel with a 13 mm $\times$ 0.2 mm rectangular cross-section, which acted as a spring. The rectangular cross-section of the spring resulted in a 1 degree of freedom (1DOF) system, which could oscillate in the direction perpendicular to the incoming flow (CF direction). The upper end of the spring was clamped to a fixed support. This design made it possible to obtain 1DOF oscillations without any need for an air bearing system, which would add to the moving mass of the system, and would have made it impossible to observe any oscillations at low Reynolds numbers. The submerged length of the cylinder and the distance from the free end of the cylinder to the bottom of the water channel were $107D$ and $3D$, respectively. These distances were kept constant for all experiments. The reduced velocity of the system was changed by changing the natural frequency of the system, instead of changing the flow velocity. The natural frequency of the system was changed by changing the length of the spring. This length was adjusted by fixing a collar that could move on a vertical column placed next to the spring at desired locations (figure 1*a*). The obtained natural frequency was inversely proportional to the square of the spring's length.

The amplitude of oscillations was measured using a high-resolution distance measuring laser (Panasonic HL-G112) which recorded displacements at a known location on the spring close to the point where the spring was attached to the cylinder. Then based on these measurements, the displacement at the tip of the cylinder was determined using similar triangles that were created with the measured displacement and the fixed upper end of the spring, and the tip displacement and the fixed upper end of the spring. These measurements were also validated by comparing the amplitude of tip oscillations with the amplitude obtained based on tracking the lower end of the cylinder during its oscillations using the high-speed camera footage. These measurements were reported as the dimensionless oscillation amplitude, $A^* = A/D$. The oscillation amplitude, A, was found as the magnitude of the peak of the fast Fourier transform (FFT) of the displacement time histories.

The system's natural frequency in air and its corresponding damping ratio were measured using a decay test. An initial displacement of approximately $5D$ was given to the cylinder and the oscillations were recorded for over 30 seconds. The natural frequency was then determined by finding the peak frequency of the resulting oscillations. The damping ratio, ζ, was calculated by fitting an exponentially decaying curve to the peak amplitudes of the measured oscillations. For the tests at a constant Reynolds number, the mass ratio, m^*, defined as the ratio between the moving mass and the mass of displaced water, was varied from 3.8 to 5.1 over the lock-in range, and ζ decreased from 0.003 to 0.002, resulting in a mass-damping coefficient of $m^*\zeta = 0.01$ for the entire lock-in range. For the tests with a variable Reynolds number, the mass ratio stayed constant at $m^* = 6.9$, and the damping ratio was $\zeta = 0.003$, resulting in a mass-damping coefficient of $m^*\zeta = 0.021$.

The flow around the cylinder was visualized using PIV. Neutrally buoyant glass spheres with a diameter of 50 microns were added to the water in the water channel and mixed until the spheres were evenly distributed. A laser plane was then created parallel to the bottom

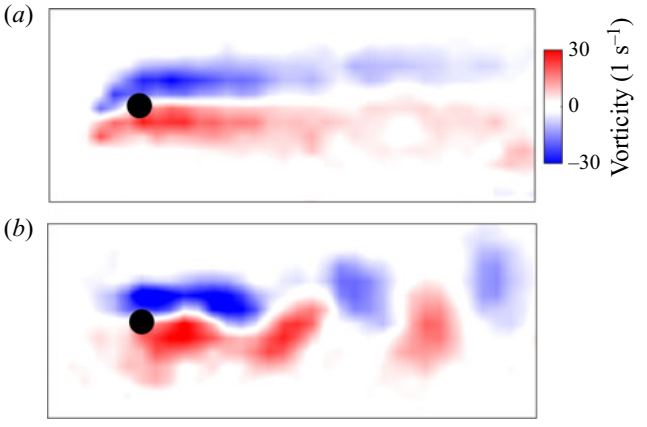

Figure 2. The wake of a fixed cylinder at (*a*) $Re = 33$ and (*b*) $Re = 60$.

of the water channel and located close to the tip of the cylinder. This plane illuminated a 2-D cross-section of the flow around and in the wake of the cylinder. A high-speed camera (Phantom V4.2 at 300 f.p.s. and 1280 × 960 resolution) was used to record the flow around the cylinder through the clear bottom of the water channel (figure 1*a*). An open source PIV analysis tool for MATLAB, PIVlab v2.38, was used to analyse images recorded by the camera and calculate the flow velocities and vorticities.

3. Results

3.1. *The wake of a fixed cylinder*

In order to validate our experimental set-up, we conducted flow visualizations to observe the wake of a fixed cylinder at Reynolds numbers below and above the critical Reynolds number, $Re_{cr} = 47$. Figure 2 shows two sample cases for $Re = 33$ (smaller than $Re_{cr} = 47$), and $Re = 60$ (larger than $Re_{cr} = 47$). In the case of $Re = 33$ (figure 2*a*), the shear layers are observed in the wake; however, they do not interact with each other and as a result, no shedding of vortices is observed, as expected. For the case of $Re = 60$ (figure 2*b*), the shear layers that are observed in the wake do interact, and vortex shedding is observed in the wake, as expected for a case with a Reynolds number larger than the critical.

3.2. *Subcritical VIV at a constant Reynolds number*

We conducted experiments using our flexibly mounted cylinder set-up at four different constant Reynolds numbers: $Re = 17$, 19, 22 and 33. For each Reynolds number, we varied the reduced velocity by changing the length of the spring, while keeping the flow velocity constant. This method of changing the stiffness resulted in change in the system's mass ratio, m^*. As the spring became longer to decrease the natural frequency (and increase the reduced velocity), the moving mass was increased, and as a result the added mass was increased over the lock-in range from $m^* = 3.8$ to $m^* = 5.1$. For each test, the cylinder was given an initial displacement of approximately $1D$. After waiting for 3 min for the transient response to decay, the steady-state response of the system was measured for 2 min.

Figure 3 shows the dimensionless amplitude and frequency of the response vs the reduced velocity for all four cases. The error bars shown in the plots of figure 3, and in the

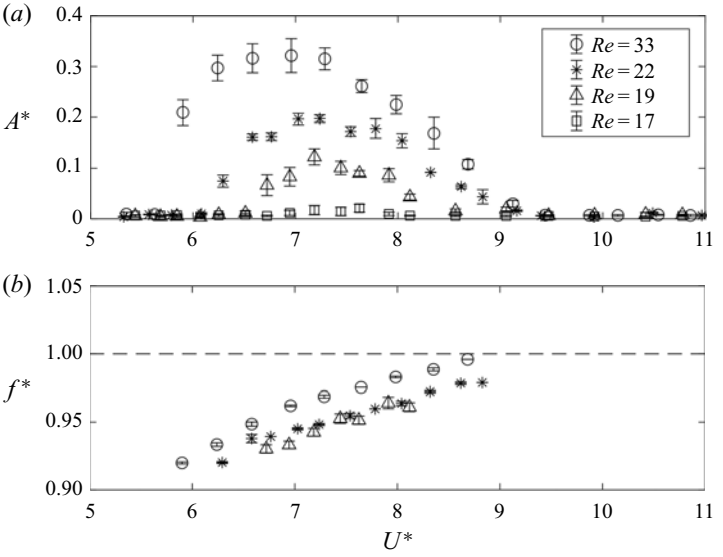

Figure 3. (*a*) The dimensionless amplitude and (*b*) the dimensionless frequency of the response for a flexibly mounted cylinder at constant subcritical Reynolds numbers. The error bars are standard deviations of the calculated values from at least three independent runs of each test.

similar plots that will follow, are standard deviations of the calculated values from at least three independent runs of each test. As observed in figure 3(*a*), except for $Re = 17$, which does not exhibit any steady-state oscillatory motion, at all other Reynolds numbers VIV is observed. At $Re = 19$, VIV starts at $U^* \approx 6.5$ and ends at $U^* \approx 8.6$, and the maximum amplitude of oscillations observed is $A^* \approx 0.12$. As the Reynolds number is increased, the range of reduced velocities over which VIV is observed and the amplitude of oscillations increase. The widest lock-in range is observed at $Re = 33$ for a reduced velocity range of $U^* = 5.8$–9.2. The largest amplitude of oscillations observed in these series of tests is $A^* \approx 0.32$ and is observed for $Re = 33$. For all three Reynolds numbers where oscillations are observed, the frequency of oscillations stays slightly lower than the natural frequency of the system (figure 3*b*). This is similar to what Mittal & Singh (2005) observed in their numerical results. As discussed by Mittal & Singh (2005) and Williamson & Govardhan (2004), this difference between the two frequencies is due to the small mass ratio of the system. Mittal & Singh (2005) showed numerically that for small mass ratios, the oscillation frequency during the lock-in range remains lower than the natural frequency of the system, and as the mass ratio is increased, the oscillation frequency approaches the natural frequency.

The maximum amplitude of oscillations and the width of lock-in range observed by Mittal & Singh (2005) for $Re = 33$ are $A^* = 0.43$ and $U^* = 5.5$–10.5, respectively, which are comparable with the values we have observed in the present experiments: a maximum amplitude of oscillations of $A^* = 0.32$ and a lock-in range of $U^* = 5.8$–9.2. The slight differences in these values could be due to several differences between the numerical and experimental set-ups: the numerical results have zero structural damping, while the experimental results do have small but non-zero structural damping; the mass ratios of the experimental and numerical results are similar, but not exactly the same, and the cylinder used in the experiments had pendulum-like oscillations, while the numerical results have been for a two-dimensional case.

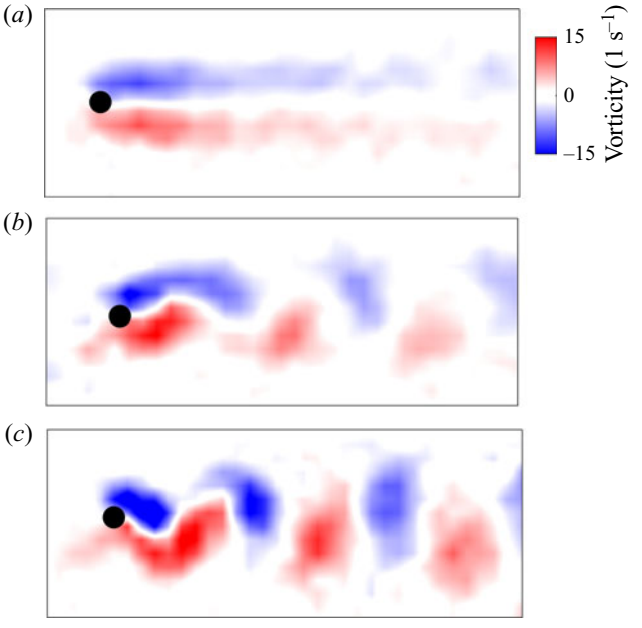

Figure 4. The wake of a flexibly mounted cylinder at a fixed reduced velocity, $U^* = 7.5$, and three sample subcritical Reynolds numbers: (*a*) $Re = 17$, (*b*) $Re = 22$ and (*c*) $Re = 33$.

The wake of the flexibly mounted cylinder is shown in figure 4 at a constant reduced velocity of $U^* = 7.5$, and for three different Reynolds numbers: $Re = 17$, 22 and 33. Recall from figure 3 that oscillations are observed for $Re = 22$ and 33, but not for $Re = 17$. It is clear in figure 4 that vortex shedding is observed for $Re = 22$ and 33, but not for $Re = 17$, confirming that vortex shedding is observed in the wake of the cylinder when oscillations are observed. The shedding frequencies at $Re = 22$ and 33 are equal to 2.6 ± 0.1 Hz and 4.3 ± 0.1 Hz, respectively, which are the same as the oscillation frequencies at these Reynolds numbers, as expected for reduced velocities within the lock-in range where synchronization has occurred between the cylinder's oscillations and the shedding of vortices in its wake. The differences in the wake between figures 2(*a*) and 4(*c*) clearly show how, for $Re = 33$, no shedding is observed in the wake of a fixed cylinder, and shedding is observed when the cylinder undergoes VIV. For $Re = 17$ (figure 4*a*), on the other hand, two shear layers are observed in the wake, with no interaction between them, and as a result no shedding is observed. The wake of a flexibly mounted cylinder at $Re = 17$ (figure 4*a*) is similar to the wake of a fixed cylinder at any subcritical Reynolds number, such as that shown in figure 2(*a*) for $Re = 33$.

3.3. *Increasing the Reynolds number at a constant reduced velocity*

A question that arises after observing the results of figure 3 is: Up to which Reynolds number will the amplitude of the observed VIV response increase? Since the amplitude of the VIV response at postcritical Reynolds numbers does not depend significantly on the Reynolds number, it is expected that by increasing the Reynolds number in the subcritical range, at some point, the amplitude reaches a plateau. To investigate the existence of a plateau in these experimental results, we held the reduced velocity constant at $U^* = 7.5$ and varied the Reynolds number within the subcritical range. This choice of the reduced

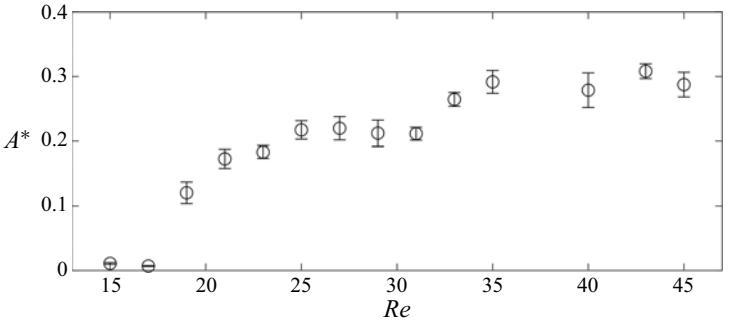

Figure 5. Dimensionless amplitude response of a flexibly mounted cylinder at a constant reduced velocity of $U^* = 7.5$ for varying Reynolds numbers.

velocity was because at $U^* = 7.5$ we have observed VIV at all three Reynolds numbers of figure 3, and also the observed amplitude at $U^* = 7.5$ is close to the maximum amplitude observed for each constant-Reynolds-number case. Figure 5 shows that the VIV amplitude increases initially with increasing Reynolds numbers, as also observed in the results of figure 3(*a*), but then reaches a plateau for $Re > 33$, where the VIV amplitude remains close to a value of $A^* \approx 0.31$ for higher subcritical Reynolds numbers.

3.4. *Subcritical VIV for variable Reynolds numbers*

Besides the experiments at constant subcritical Reynolds numbers, we conducted a series of experiments in which we varied the reduced velocity in the way that is typically done in experimental studies on VIV: by keeping the natural frequency of the system constant and increasing the flow velocity, and therefore increasing the Reynolds number within the lock-in range. In these experiments, we selected the natural frequency such that at $Re = 22$, the reduced velocity would be equal to the critical reduced velocity at which oscillations began for the constant-Reynolds-number case of $Re = 22$. This means that the reduced velocity that corresponds to the beginning of the lock-in range is the same for the tests with constant Reynolds number at $Re = 22$ and this series of variable-Reynolds-number tests. We selected $Re = 22$ as the Reynolds number at the onset of the lock-in range to ensure that the Reynolds number for the entire lock-in range stays within the subcritical range.

Figure 6 shows the dimensionless amplitudes of oscillations for the constant-Reynolds-number and variable-Reynolds-number cases vs reduced velocity. The Reynolds number in the case of the variable Re varies from $Re = 22$ to 34 within the lock-in range. While the width of the lock-in range does not change, the amplitudes of oscillations for the case of the variable Reynolds number are consistently larger than those for the constant Reynolds number, except for the very first point in the lock-in range for which $Re = 22$ for both sets of data. This increase in the amplitude is expected, as we previously observed in figures 3 and 5 that increasing Reynolds number over this range results in an increase in the amplitude of oscillations. Despite this difference, the results of figure 6 confirm that subcritical VIV can be observed for variable Reynolds numbers as well, as also observed numerically by Mittal & Singh (2005).

3.5. *The influence of mass ratio*

In the experiments with a constant Reynolds number (figure 3), the mass ratio did not stay constant. In order to investigate whether or not this increase in the added mass influences

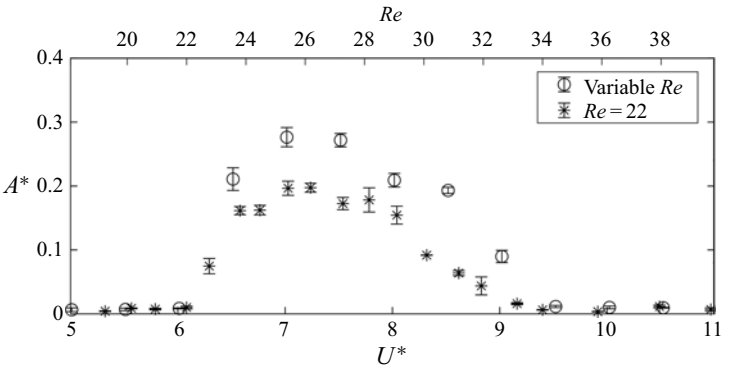

Figure 6. Dimensionless amplitude response of a flexibly mounted cylinder vs reduced velocity for a constant Reynolds number of $Re = 22$, as well as a case of variable Reynolds number within the lock-in range.

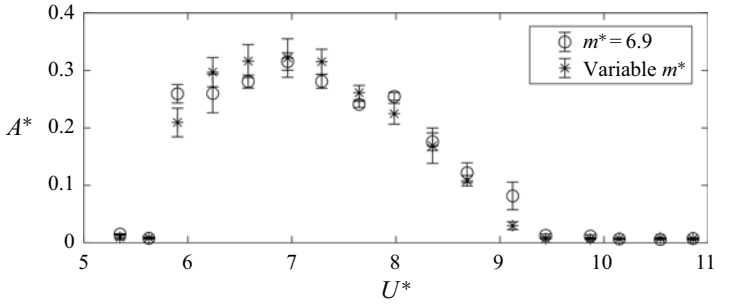

Figure 7. Dimensionless amplitude response of a flexibly mounted cylinder at a constant Reynolds number of $Re = 33$ with varying or constant mass ratios.

the observed results, we conducted a series of tests in which we kept the mass ratio constant, while keeping the Reynolds number constant as well at $Re = 33$. In order to keep the mass ratio constant, we attached several pieces of magnet close to the clamped end of the spring. Each of these magnetic pieces had a mass equal to the change in moving mass every time the length of the spring was varied to adjust the natural frequency. As a result, for each step, when the collar was moved to a new location, we removed one of these magnetic pieces and kept the total moving mass constant for all reduced velocities. This ensured that the mass ratio remained constant at $m^* = 6.9$.

Figure 7 shows the amplitude plots for the VIV response of the system with a constant mass ratio and the system that we discussed earlier in figure 3 with a variable mass ratio, both at the same Reynolds number of $Re = 33$. The mass ratio for the variable-mass-ratio case varied from $m^* = 3.7$ to $m^* = 5.1$ within the lock-in range. It is clear from the results shown in figure 7 that very similar amplitudes of oscillations and lock-in ranges are observed for both cases, implying that the change in the mass ratio over the lock-in range does not influence the observed VIV response.

4. Conclusions

We have presented experimental evidence of the existence of VIV in subcritical Reynolds numbers for the first time, confirming what had been obtained numerically and theoretically in the past (Mittal & Singh 2005; Kou *et al.* 2017; Dolci & Carmo 2019).

To be able to conduct these experiments, we designed and built a rotating water channel together with a mounting mechanism that enabled conducting VIV experiments at low and constant Reynolds numbers.

In these experiments, the VIV is observed at fixed subcritical Reynolds numbers as low as $Re = 19$. This Reynolds number is very close to what was shown previously (Kou *et al.* 2017) to be the minimum Reynolds number for observing subcritical von Kármán shedding in the wake of a cylinder (i.e. $Re = 18$). The amplitude of oscillations as well as the width of the lock-in range increase with increasing Reynolds number. For a fixed reduced velocity, the amplitude of oscillations increases with increasing Reynolds number and approaches a plateau for $Re > 33$. This is in agreement with the previous results of VIV experiments at larger Reynolds numbers, for which the amplitude of observed oscillations was shown to be independent from the Reynolds number. Wake visualizations reveal that while, in agreement with previous studies, no shedding is observed in the wake of a fixed cylinder at subcritical Reynolds number in our experiments, for the case of a flexibly mounted cylinder, shedding is observed at all subcritical Reynolds numbers for which oscillations are observed. The shedding frequency for all these cases is equal to the oscillation frequency, suggesting that lock-in has occurred. These experimental results also confirm that subcritical VIV can be observed for the case where the Reynolds number is varied within the lock-in range, while staying within the subcritical range, as well. Despite slight quantitative differences between the amplitudes of oscillations in subcritical VIV at constant Reynolds number and subcritical VIV with variable Reynolds number, the main features of a VIV response are observed in both cases.

Acknowledgements. The authors are grateful to Mr U. Patel for helping with the design and manufacturing of the water channel used in these experiments.

Funding. This work was partially supported by the National Science Foundation under grant CBET-1705251.

Declaration of interests. The authors report no conflict of interest.

Author ORCIDs.
Jonathan P. Rothstein https://orcid.org/0000-0003-3214-6365;
Yahya Modarres-Sadeghi https://orcid.org/0000-0002-7890-1699.

References

Bourguet, R. 2020 Vortex-induced vibrations of a flexible cylinder at subcritical Reynolds number. *J. Fluid Mech.* **902**, R3.

Buffoni, E. 2003 Vortex shedding in subcritical conditions. *Phys. Fluids* **15**, 814–816.

Dolci, D.I. & Carmo, B.S. 2019 Bifurcation analysis of the primary instability in the flow around a flexibly mounted circular cylinder. *J. Fluid Mech.* **880**, R5.

Kou, J., Zhang, W., Liu, Y. & Li, X. 2017 The lowest Reynolds number of vortex-induced vibrations. *Phys. Fluids* **29**, 041701.

Mathis, C., Provansal, M. & Boyer, L. 1984 The Bénard–von Kármán instability: an experimental study near the threshold. *J. Phys. Lett.* **45** (10), 483–491.

Mittal, S. & Singh, S. 2005 Vortex-induced vibrations at subcritical *Re*. *J. Fluid Mech.* **534**, 185–194.

Païdoussis, M.P., Price, S.J. & De Langre, E. 2010 *Fluid-Structure Interactions: Cross-Flow-Induced Instabilities*. Cambridge University Press.

Sarpkaya, T. 2004 A critical review of the intrinsic nature of vortex-induced vibrations. *J. Fluids Struct.* **19**, 389–447.

Williamson, C. & Govardhan, R. 2004 Vortex-induced vibrations. *Annu. Rev. Fluid Mech.* **36**, 413–455.